

Phonon-plasmon coupling in electron surface accumulation layers in InN nanocolumns

S. Lazić, E. Gallardo, and J. M. Calleja

Departamento de Física de Materiales, Universidad Autónoma de Madrid, E-28049 Madrid, Spain

F. Agulló-Rueda

Instituto de Ciencia de Materiales de Madrid, CSIC, E-288049 Madrid, Spain

J. Grandal, M. A. Sánchez-García, and E. Calleja

ISOM and Departamento de Ingeniería Electrónica, ETSIT, Universidad Politécnica de Madrid, E-28040 Madrid, Spain

E. Luna and A. Trampert

Paul-Drude-Institut für Festkörperelektronik, Hausvogteiplatz 5-7, D-10117 Berlin, Germany

(Received 22 July 2007; revised manuscript received 10 October 2007; published 20 November 2007)

Raman measurements in high quality InN nanocolumns display a coupled LO phonon-plasmon mode together with uncoupled phonons. The coupled mode is attributed to the spontaneous accumulation of electrons on the lateral surfaces of the nanocolumns. For increasing growth temperature, the electron density decreases as the growth rate increases. The present results indicate that electron accumulation layers do not only form on polar surfaces of InN but also occur on nonpolar ones. According to recent calculations, we attribute the electron surface accumulation to the temperature dependent In-rich surface reconstruction on the nanocolumn sidewalls.

DOI: [10.1103/PhysRevB.76.205319](https://doi.org/10.1103/PhysRevB.76.205319)

PACS number(s): 73.20.At, 73.22.-f, 78.30.Fs, 78.67.Bf

I. INTRODUCTION

Nanostructures based on group-III nitrides are being the object of increasing attention for basic physics and novel applications, such as strong light-matter coupling in microcavities^{1,2} or high-temperature single photon emitters in the ultraviolet range.³ Among group-III nitrides, InN is interesting because it extends the range of applications to the visible and infrared (IR) spectral region. Also, the small electron effective mass of InN is promising for high speed device applications. InN-based nanostructures are not abundant because of their specific growth difficulties⁴ (mainly due to the InN low dissociation temperature) and the poorer knowledge of InN fundamental parameters, as compared to other nitrides. Indeed, InN is being the object of controversy due to the ubiquitous presence of high electron concentrations, whose origin (unintentional doping, interface effects, or surface accumulation) is still under discussion. Thus, the Burstein-Moss shift produced by the high electron densities has prevented until recently the determination of the band gap edge^{5,6} of InN. Free electrons also affect the phonon spectrum of InN, as the longitudinal optical (LO) phonons couple with electrons producing coupled phonon-plasmon excitations.⁷ Coupled modes in InN films have been studied by several groups^{8–14} using Raman scattering, IR reflectance, and IR ellipsometry.¹¹ Infrared and Raman scattering measurements in InN nanocolumns (NCs) have also been reported recently.¹⁵ The apparent coexistence of uncoupled LO modes and coupled (L_+ , L_-) ones is still the object of debate. An L_- mode in the range of 400–450 cm^{-1} depending on electron density has been reported^{8,9} in InN films, coexisting with the uncoupled $A_1(\text{LO})$ phonon at 586 cm^{-1} . To explain this coexistence, surface or interface depletion layers have been invoked, where the uncoupled $A_1(\text{LO})$ phonon could

exist.¹⁰ However, IR ellipsometry measurements¹¹ showed that this hypothetical depletion layer would be too thin to be responsible for the strong LO modes observed. Alternatively, the mode observed at the $A_1(\text{LO})$ frequency has been attributed to a coupled phonon-plasmon mode shifted to high energies by wave vector nonconservation during the scattering process.^{11–14} The origin of the massive failure of wave vector conservation required for this explanation implies significant crystalline disorder,¹⁴ being difficult to understand in samples with high crystalline quality and no intentional doping. This is especially true for samples where long uniform nanocolumns⁴ or nanorods^{15,16} are formed, which are practically free of defects. Recent measurements of inelastic electron scattering,¹⁷ Hall resistance¹⁸ and angle-resolved photoemission spectroscopy¹⁹ indicate the presence of an intrinsic electron accumulation layer on the surface of InN films. Electrons accumulate because the conduction band minimum of InN at the Γ point lies below the branch-point energy E_B (or the average midgap energy across the entire Brillouin zone).¹⁷ This results in the ionization of surface donor states and a downward band bending at the surface, where electrons accumulate. A recent theoretical work²⁰ confirms that electron accumulation occurs on the polar surfaces of InN. In this context, the presence of a high surface electron concentration seems to be an intrinsic characteristic of InN rather than a result of imperfect growth or accidental doping. With this in mind, the effect of an inhomogeneous electron distribution on the phonon-plasmon coupled modes has to be revised.

In this paper, we report on inelastic light scattering measurements on both compact and nanocolumnar InN high quality samples. The NC samples show a low-energy LO phonon-plasmon coupled mode (L_-) in the 425–450 cm^{-1} range, which is not observed in our compact samples, probably due to their comparatively low specific surface. The

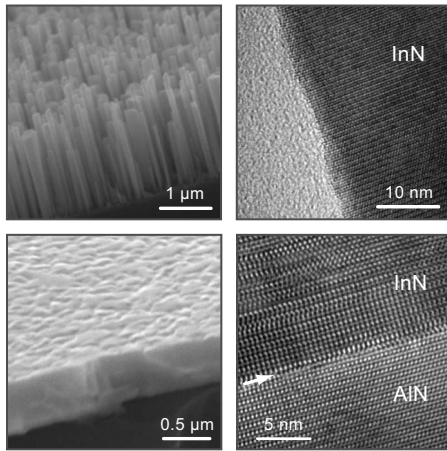


FIG. 1. Typical SEM (left) and HRTEM (right) images of nanocolumnar (top) and compact (bottom) InN samples.

corresponding plasma frequency gives electron concentrations in the range from 2.5×10^{18} to $6.0 \times 10^{18} \text{ cm}^{-3}$. These values agree reasonably with the plasma resonance observed in the IR-reflectance spectra of the NC. Our results suggest that the electron concentration at the NC sidewalls gives rise to coupled modes, while the uncoupled (or weakly coupled to the background electrons) LO phonon originates from the underlying regions inside the NC.

II. EXPERIMENT

InN films were grown on Si(111) (Ref. 21) and Si(001) substrates by plasma-assisted molecular beam epitaxy. A 50 nm thick AlN buffer layer was used to optimize growth conditions of samples grown on Si(111). Details about the growth system can be found in Ref. 21. The III/V ratio was varied from N-rich conditions (NC samples) to quasistoichiometry (compact samples). The growth temperature was varied between 450 and 480 °C. Scanning electron microscopy (SEM) and high resolution transmission electron microscopy (HRTEM) cross-sectional images were obtained to determine the morphology and structure of the samples. The SEM pictures displayed in Fig. 1 correspond to samples grown on Si(111). They reveal the NC morphology typical for N-rich growth conditions⁴ (top left) and the compact film obtained in quasistoichiometric conditions (bottom left). The HRTEM pictures in the right panels show the excellent crystalline quality of the nanocolumns (top right) together with the abruptness of the AlN-InN interface (marked by an arrow) of the compact sample (bottom right). The NCs are hexagonal prisms with their axis oriented parallel to the growth direction.⁴ NCs grown on Si(001) substrates show a slight orientation disorder compared to those grown on Si(111). No significant differences in the Raman spectra were found between NC grown along both substrate directions. Raman scattering experiments were carried out at room temperature, both in macro- and microconfigurations using a He-Ne and Ar⁺-ion laser for excitation. The scattered light was dispersed by both single- (SPEX 750M) and double-grating spectrometers (SPEX Model 1404) with a charge coupled device de-

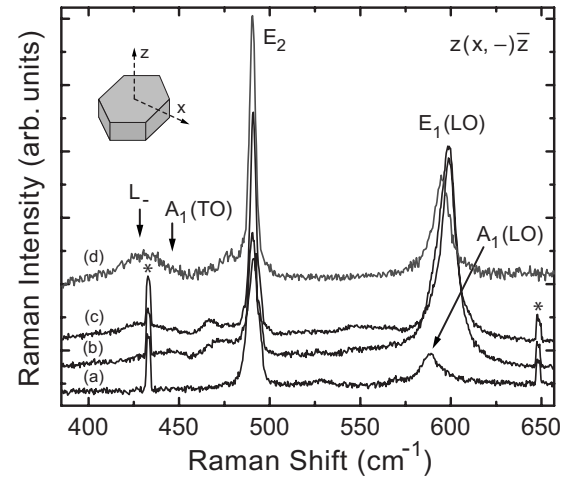


FIG. 2. Room-temperature macro-Raman spectra of a compact layer (lower trace) and two NC samples grown on Si(111) at 460 °C (middle trace) and 475 °C (upper trace) for $z(x, -)\bar{z}$ nominal scattering configuration. The inset shows the scattering directions relative to the crystal structure. Ne plasma lines (marked with asterisks) are used for wave number calibration.

detector. The spectra were taken in nominal backscattering configurations, both along the growth direction (c axis) and perpendicular to it (from the lateral sample surface). The experiments have been carried out with a spectral resolution of typically 2 cm^{-1} . A $100\times$ microscope objective was used to focus the laser beam to spot size of typically $<2 \mu\text{m}$ diameter. The photoluminescence (PL) measurements were performed at low temperature (15 K) using the 488 nm line of an Ar⁺-ion laser as an excitation source. The PL signal was focused into a 85 cm focal length monochromator, detected by a liquid nitrogen cooled Ge photodetector and processed using standard lock-in techniques. The PL spectra were corrected by the system-detector response curve. The IR spectra were recorded at room temperature with a Bruker IFS66v spectrometer, covering a frequency range of $560\text{--}7000 \text{ cm}^{-1}$. Each spectrum contains 200 scans with an instrumental resolution of 2 cm^{-1} .

III. RESULTS AND DISCUSSION

The macro-Raman spectra recorded in backscattering configuration along the c axis are shown in Fig. 2 for a compact film grown at (a) 475 °C and two NC samples grown at (b) 460 °C and (c) 475 °C on Si(111). Spectra (a)–(c) correspond to 632.8 nm excitation. Spectrum (d) of the same sample as in (c) is excited at 514.5 nm. The scattering directions relative to the crystalline structure are shown in the inset. The z direction is parallel to the hexagonal axis and the x and y directions are mutually orthogonal and have arbitrary orientations in the plane normal to z . The phonon frequencies have been carefully determined using Ne spectral lines for calibration.

For 632.8 nm excitation, the compact sample shows the allowed E_2 (491 cm^{-1}) and $A_1(\text{LO})$ (588 cm^{-1}) modes. These values differ from the ones reported by Davydov

et al.^{8,9} but coincide with other reported in several publications (see Ref. 9 and references therein). The discrepancy in InN phonon frequencies reported in the literature can be due to different amounts of deformation (residual and thermal strain) and the presence of structural defects in InN layers. The small width (4.0 cm^{-1}) of the nonpolar E_2 mode confirms the high crystalline quality observed by HRTEM. The NC samples show an equally narrow E_2 peak at essentially the same frequency. However, the LO mode appears at the $E_1(\text{LO})$ frequency (600 cm^{-1} for 632.8 nm and 596 cm^{-1} for 514.5 nm excitations), which is forbidden in this scattering geometry. The changes in the LO phonon frequency for different excitation wavelengths are observable in Fig. 2. They are attributed to changes in the penetration depth of the incoming light. The same behavior was reported in Ref. 22 and speaks against the dispersion of the phonon-plasmon coupled mode which would result in a decrease of the mode frequency with increasing excitation wavelength.²³ This indicates that the mode observed at the $E_1(\text{LO})$ frequency cannot be attributed to a coupled phonon-plasmon mode shifted to higher wave numbers by wave vector nonconservation during the scattering process. The change in the LO frequency with excitation wavelength could therefore reflect the changes in the free carrier concentration through the NC thickness due to the different probing depths.²² Besides, the small E_2 phonon width remains practically unchanged for increasing energy of the incident photon. This excludes any significant breakdown in the wave vector conservation due to crystalline disorder.

Considering the sample morphology and the results presented below, we attribute the LO mode of the NC to the true, essentially uncoupled $E_1(\text{LO})$ phonon. Its appearance is due to the light refraction and/or scattering at the lateral surfaces of the NC. As a result of the comparatively high specific surface of the NC samples and the finite aperture of the collection optics, together with the high refraction index of InN (Ref. 24) around 2.9, most of the light enters through (and scatters from) the lateral surfaces of the nanocolumns. This results in a phonon propagation direction close to perpendicular to the c axis, i.e., of quasi- E_1 symmetry. To confirm this assignment, we performed micro-Raman measurements in $x(y, -)\bar{x}$ scattering configuration from the lateral surface of the samples. Figure 3 shows the spectra of the compact layer and the NC grown at 475 °C on Si(111). Besides the strong peak of the Si substrate at 521 cm^{-1} , the $E_1(\text{LO})$ phonon appears at 600 cm^{-1} in both samples. This demonstrates that the light propagates essentially perpendicular to the NC sidewalls, irrespective of the nominal scattering geometry. We have observed the same effect in GaN NC when compared to GaN compact layers. The deviation of the light propagation in NC depends on the degree of “surface roughness” due to the inhomogeneity of column height or column density in different samples. Samples with higher NC density and height homogeneity will show smaller deviations. Although not specifically reported by other authors, the “anomalous” light propagation in NC might be a general fact. Thus, the $E_1(\text{LO})$ mode at 740 cm^{-1} systematically appears in nominal backscattering along the c axis in the spectra of GaN nanocolumns.^{25,26} Also, the Raman spectra re-

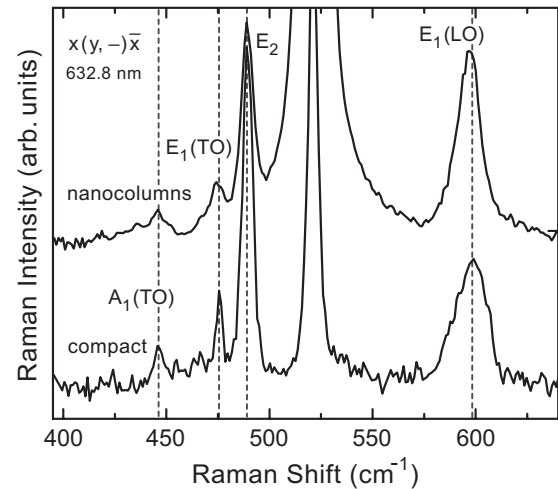


FIG. 3. Room-temperature micro-Raman spectra of the compact layer and the NC sample grown on Si(111) at 475 °C taken in backscattering at the lateral surface.

ported in Fig. 3 of Ref. 15 show a small ($3\text{--}4 \text{ cm}^{-1}$) shift to higher frequency of the LO phonon of InN NC samples as compared to a reference thick film. This shift amounts to one-half of the $E_1(\text{LO})$ - $A_1(\text{LO})$ splitting in InN, thus indicating a significant deviation of the phonon propagation direction from the c axis. In the low frequency region of Fig. 3, the two TO modes are observed in both samples, as no polarization of the scattered light has been selected. The feature appearing near 468 cm^{-1} in the NC samples excited at 632.8 nm [Fig. 2(c)] is absent for 514.5 nm excitation [Fig. 2(d)]. As the InN band structure has no critical points in this energy range, we attribute this feature to an extrinsic effect.

Considering that the lateral surfaces of the nanocolumns provide the main contribution to the light scattering, we attribute the broad peak observed in the $425\text{--}450 \text{ cm}^{-1}$ range in NC samples (Fig. 2) to the low-energy branch L_- of the coupled LO phonon-plasmon mode arising from an electron accumulation layer at the lateral surfaces of the NC. [Incidentally, the L_- peak cannot be confused with the $A_1(\text{TO})$ phonon. As the dispersion of $A_1(\text{TO})$ phonons away from the Brillouin zone center is positive in wurtzite, scattering events without wave vector conservation would result in a peak at higher frequencies than the zone-center one⁸ (447 cm^{-1} , marked in Fig. 2).] Consequently, the uncoupled $E_1(\text{LO})$ phonon must arise from the inner part of the NC, where the electron density is expected to be much smaller.^{17–19} The dependence of the intensity ratio of the L_- to the $E_1(\text{LO})$ peak on the excitation wavelength presented in Fig. 4 supports this assignment. The strong increase of this ratio (circles) observed by changing the excitation wavelength from 632.8 to 457.9 nm could be attributed, in principle, to a change in the light penetration depth. However, the absorption coefficient of InN changes only moderately (from 1.2×10^5 to $8 \times 10^4 \text{ cm}^{-1}$) (Ref. 9) in this wavelength range. Assuming a thickness of the accumulation layer at the NC sidewalls similar to that reported for polar surfaces [$\leq 5 \text{ nm}$ (Refs. 17 and 19)], and taking the average NC diameter as 100 nm (see Fig. 1), the expected change of the L_- to the

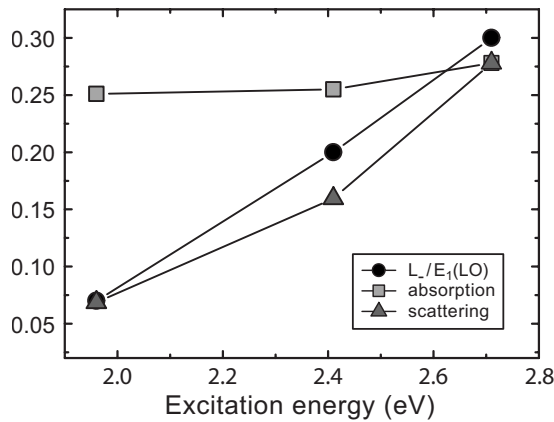


FIG. 4. The intensity ratio of the L_- to the $E_1(\text{LO})$ peak versus excitation wavelength (circles) for the NC sample grown at 475 °C. The expected change of the L_- to the $E_1(\text{LO})$ intensity ratio due to the change in the absorption coefficient (squares). Fourth power of the excitation energy normalized to 1.95 eV (triangles).

$E_1(\text{LO})$ intensity ratio due to the change in the absorption coefficient (α) is very small, as shown by the squares in Fig. 4. However, considering that the typical roughness of the NC sample is of the order of the wavelength [see Fig. 1 (top left)], strong light scattering is expected to occur. Light scattering enhances the surface contribution of the total light emission, and its intensity decays as the fourth power of the exciting wavelength λ . The triangles in Fig. 4 represent λ^{-4} normalized to the lowest energy (1.95 eV) point. Consequently, the observed increase of the L_- to the $E_1(\text{LO})$ intensity ratio for decreasing excitation wavelength is likely to be due mainly to scattering at the NC surfaces. Electron accumulation at the sidewalls of InN NC has been reported recently by transport measurements on single NC²⁷ and photoluminescence measurements of the valence band minimum to surface Fermi level separation for a -plane InN.²⁸

The presence of free electrons in the NC is confirmed by infrared reflectance measurements, shown in Fig. 5, for the compact and the NC sample grown on Si(111) at 475 °C. A detailed fit of the reflectance spectra is difficult considering the sample geometry. However, the strong reflectance mini-

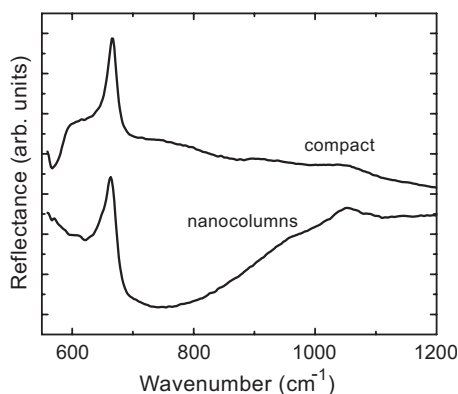


FIG. 5. Infrared-reflectance spectra of the compact layer and the NC sample grown at 475 °C.

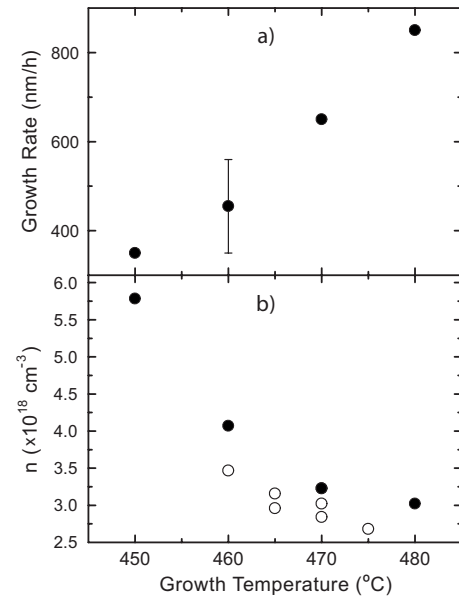


FIG. 6. (a) Growth rate of NC samples grown on Si(001) versus growth temperature. (b) Electron concentration versus growth temperature obtained from the L_- frequency. Full symbols stand for NC samples grown on Si(001) substrates; open symbols for Si(111) ones.

um in the NC sample in the 700–800 cm^{-1} region is indicative of absorption by free electrons. The plasma frequency ω_p corresponding to the observed L_- frequency can be estimated from the simplest model for the dielectric function,²⁹

$$L_{\pm}^2 = \frac{1}{2} \{ \omega_{\text{LO}}^2 + \omega_p^2 \pm [(\omega_{\text{LO}}^2 + \omega_p^2)^2 - 4\omega_{\text{TO}}\omega_p^2]^{1/2} \}, \quad (1)$$

where ω_{LO} and ω_{TO} are the longitudinal and transverse optical phonon frequencies. The corresponding L_+ modes should appear in the 950–1300 cm^{-1} region. They are not observed, probably due to damping. Taking $\omega_{\text{LO}} = 600 \text{ cm}^{-1}$ and $\omega_{\text{TO}} = 476 \text{ cm}^{-1}$ (Ref. 8) and assuming an effective mass³⁰ $m^* = 0.05m_0$ and an optical dielectric constant¹¹ $\epsilon_{\infty} = 6.7$, we can estimate the electron concentration n from Eq. (1) and the plasma frequency $\omega_p^2 = ne^2/m^* \epsilon_{\infty}$ (with m_0 and e being the free-electron mass and charge, respectively). Its values for all samples studied are presented in Fig. 6(b) as a function of the growth temperature, together with the corresponding changes in the growth rate [Fig. 6(a)]. One observes a marked decrease of the electron concentration estimated from the L_- frequency for increasing growth temperature for NC samples grown on both Si(111) substrates (open symbols) and Si(001) ones (full symbols). We tried to confirm the change of the electron density observed in Fig. 6(b) by photoluminescence and IR-reflectance measurements. Reflectance results were not conclusive, perhaps due to the variable morphology of the different samples and the longer wavelengths involved, which result in a larger penetration depth and reduced scattering. As for PL, the low-temperature results for NC samples grown on Si(111) at 475 and 460 °C are displayed in Fig. 7. PL spectra show a pronounced

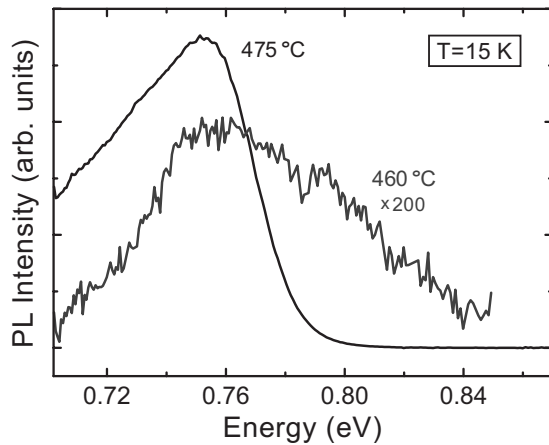


FIG. 7. Low-temperature PL spectra of NC samples grown on Si(111) at 475 and 460 °C.

Burstein-Moss shift to higher energies with respect to the band gap of InN.³¹ The PL band shape differs for the samples grown at different temperatures. The blueshift of the high-energy tail of the PL band for the sample grown at 460 °C (with respect to the one grown at 475 °C) indicates an increase in the electron concentration. For both samples, the electron concentration estimated from the shift of the Fermi level roughly coincides with the values derived from the position of the L_- mode [Fig. 6(b)]. The shoulder appearing on the high-energy side for the NC sample grown at lower temperature (Fig. 7) could indicate nonuniform spatial distribution of electrons.⁹

Going back to Fig. 6(a), one observes the growth rate increase for increasing growth temperature. This trend gives an indication of the origin of the electron accumulation layer on the lateral NC surfaces. The growth mechanism of the NC implies diffusion of the impinging In atoms along the NC sidewalls up to its top. The higher growth rate observed at higher growth temperature indicates a faster In diffusion. For a fixed In flux, the instantaneous number of In atoms “climbing” up the NC is smaller as their speed increases. Consequently, at higher growth temperature, the “instantaneous In coverage” of the lateral NC surfaces decreases. This coverage is frozen upon sample cooling at the end of the growth process. The remaining In atoms could be incorporated into the NC to form an In-rich surface layer responsible for the electron accumulation.^{28,32} This accumulation should be proportional to the excess In atoms, and consequently, it should be higher for lower growth temperatures, as observed.

In summary, the Raman spectra of high quality InN nanocolumnar and compact layers of InN indicate that electron accumulation occurs at the nonpolar lateral surfaces of the nanocolumns. This electron layer couples with the $E_1(\text{LO})$ phonon, giving rise to the observed coupled L_- mode. The electron accumulation is probably due to the formation of an In-rich surface layer at the NC sidewalls.

ACKNOWLEDGMENTS

This work has been supported by research contracts of the Spanish Ministry of Education (MEC MAT2005-01388, NAN2004-09109-C04, TEC2004-05260-C02-02, and Consolider-CSD 2006-19) and the Community of Madrid (CAM S-0505-ESP-0200).

¹R. Butté, G. Christmann, E. Feltin, J.-F. Carlin, M. Mosca, M. Illegems, and N. Grandjean, *Phys. Rev. B* **73**, 033315 (2006).

²S. Christopoulos, G. Baldassarri, P. G. Lagoudakis, A. Grundy, A. V. Kavokin, J. J. Baumberg, G. Christmann, R. Butté, E. Feltin, J.-F. Carlin, and N. Grandjean, *Phys. Rev. Lett.* **98**, 126405 (2007).

³C. Santori, S. Götzinger, Y. Yamamoto, S. Kako, K. Hoshino, and Y. Arakawa, *Appl. Phys. Lett.* **87**, 051916 (2005).

⁴J. Grandal and M. A. Sánchez-García, *J. Cryst. Growth* **278**, 373 (2005).

⁵V. Yu. Davydov, A. A. Klochikhin, R. P. Seisyan, V. V. Emtsev, S. V. Ivanov, F. Bechstedt, J. Furthmüller, H. Harima, A. V. Mudryi, J. Aderhold, O. Semchinova, and J. Graul, *Phys. Status Solidi B* **229**, R1 (2002).

⁶J. Wu, W. Walukiewicz, K. M. Yu, J. W. Ager III, E. E. Haller, H. Lu, W. J. Schaff, Y. Saito, and Y. Nanishi, *Appl. Phys. Lett.* **80**, 3967 (2002).

⁷G. Abstreiter, M. Cardona, and A. Pinczuk, in *Light Scattering in Solids IV*, edited by M. Cardona and G. Güntherodt (Springer-Verlag, Berlin, 1984), p. 5.

⁸V. Yu. Davydov, V. V. Emtsev, I. N. Goncharuk, A. N. Smirnov, V. D. Petrikov, V. V. Mamutin, V. A. Vekshin, and S. N. Ivanov, *Appl. Phys. Lett.* **75**, 3297 (1999).

⁹V. Yu. Davydov and A. A. Klochikhin, *Semiconductors* **38**, 861 (2004).

¹⁰T. Inushima, T. Shiraishia, and V. Yu. Davydov, *Solid State Commun.* **110**, 491 (1999); T. Inushima, M. Higashiwaki, and T. Matsui, *Phys. Rev. B* **68**, 235204 (2003).

¹¹A. Kasic, M. Schubert, Y. Saito, Y. Nanishi, and G. Wagner, *Phys. Rev. B* **65**, 115206 (2002).

¹²F. Demangeot, C. Pinquier, J. Frandon, M. Gaio, O. Briot, B. Maleyre, S. Ruffenach, and B. Gil, *Phys. Rev. B* **71**, 104305 (2005).

¹³J. S. Thakur, D. Haddad, V. M. Naik, R. Naik, G. W. Auner, H. Lu, and W. J. Schaff, *Phys. Rev. B* **71**, 115203 (2005).

¹⁴J. W. Pomeroy, M. Kuball, C. H. Swartz, T. H. Myers, H. Lu, and W. J. Schaff, *Phys. Rev. B* **75**, 035205 (2007).

¹⁵H. Y. Chen, C. H. Shen, H. W. Lin, C. H. Chen, C. Y. Wu, S. Gwo, V. Yu. Davydov, and A. A. Klochikhin, *Thin Solid Films* **515**, 961 (2006).

¹⁶Z. H. Lan, W. M. Wang, C. L. Sun, S. C. Shi, C. W. Hsu, T. T. Chen, K. H. Chen, C. C. Chen, Y. F. Chen, and L. C. Chen, *J. Cryst. Growth* **269**, 87 (2004).

¹⁷I. Mahboob, T. D. Veal, C. F. McConville, H. Lu, and W. J. Schaff, *Phys. Rev. Lett.* **92**, 036804 (2004).

¹⁸H. Lu, W. J. Schaff, L. F. Eastman, and C. E. Stutz, *Appl. Phys.*

- Lett. **82**, 1736 (2003).
- ¹⁹L. Colakerol, T. D. Veal, H. K. Jeong, L. Plucinski, A. DeMasi, T. Learmonth, P. A. Glans, S. Wang, Y. Zhang, L. F. J. Piper, P. H. Jefferson, A. Fedorov, T. C. Chen, T. D. Moustakas, C. F. McConville, and K. E. Smith, *Phys. Rev. Lett.* **97**, 237601 (2006).
- ²⁰D. Segev and C. G. Van de Walle, *Europhys. Lett.* **76**, 305 (2006).
- ²¹J. Grandal, M. A. Sánchez-García, E. Calleja, E. Luna, and A. Trampert, *Appl. Phys. Lett.* (to be published).
- ²²M. Kuball, J. W. Pomeroy, M. Wintrebert-Fouquet, K. S. A. Butcher, H. Lu, and W. J. Schaff, *J. Cryst. Growth* **269**, 59 (2004).
- ²³D. Olego, A. Pinczuk, and A. A. Ballman, *Solid State Commun.* **45**, 941 (1983).
- ²⁴L. F. Jiang, W. Z. Shen, H. F. Yang, H. Ogawa, and Q. X. Guo, *Appl. Phys. A: Mater. Sci. Process.* **78**, 89 (2004).
- ²⁵D. Wang, C. C. Tin, J. R. Williams, M. Parka, Y. S. Park, C. M. Park, T. W. Kang, and W. C. Yang, *Appl. Phys. Lett.* **87**, 242105 (2005).
- ²⁶I. M. Tiginyanu, A. Sarua, G. Irmer, J. Monecke, S. M. Hubbard, D. Pavlidis, and V. Valiaev, *Phys. Rev. B* **64**, 233317 (2001).
- ²⁷E. Calleja, J. Grandal, M. A. Sánchez-García, M. Niebelschütz, V. Cimalla, and O. Ambacher, *Appl. Phys. Lett.* **90**, 262110 (2007).
- ²⁸T. D. Veal, P. D. C. King, M. Walker, C. F. McConville, H. Lu, and W. J. Schaff, *Physica B* (to be published).
- ²⁹E. Burstein, A. Pinczuk, and S. Iwasa, *Phys. Rev.* **157**, 611 (1967).
- ³⁰S. P. Fu and Y. F. Chen, *Appl. Phys. Lett.* **85**, 1523 (2004).
- ³¹V. Yu. Davydov, A. A. Klochikhin, V. V. Emtsev, D. A. Kurdyukov, S. V. Ivanov, V. A. Vekshin, F. Bechstedt, J. Furthmüller, J. Aderhold, J. Graul, A. V. Mudryi, H. Harima, A. Hashimoto, A. Yamamoto, and E. E. Haller, *Phys. Status Solidi B* **234**, 787 (2002).
- ³²D. Segev and C. G. Van de Walle, *Surf. Sci.* **601**, L-15 (2007); *J. Cryst. Growth* **300**, 199 (2007).